N93-13681

ELECTRON BEAM FLUORESCENCE MEASUREMENTS IN THE BOEING HYPERSONIC SHOCK TUNNEL*

L. L. Price and W. D. Williams
Calspan Corporation, AEDC Operations
Arnold Engineering Development Center
Arnold Air Force Base, Tennessee 37389

H. M. Powell, Consultant
Professor, Dept. of Electrical Engineering
Tennessee Technological University
Cookeville, Tennessee 38505

INTRODUCTION

A program entitled "Reacting Gas Experimental Data in Low Density Flow," which is funded by the Wright Laboratory/Flight Dynamics Directorate, is underway with the overall purpose of defining a set of standard experimental data against which the results of real gas computational codes can be evaluated. The goal of the particular task under which the present work was performed is to provide a complete characterization of the Boeing 30-in. Hypersonic Shock Tunnel (B30HST) at a selected test condition.

Initial experimental results for the flow characterization have been reported in Refs. 1-3. The measurement techniques utilized in these studies consisted of the usual (or classical) physical probes for determination of incident shock velocity, reflected shock pressure, nozzle wall static pressure, test section pitot and static pressure, and test section model heating rate. In addition, a direct measurement of free-stream velocity was made using a time- of-flight vaporizing wire technique. Nonintrusive techniques such as Rayleigh scattering for free-stream density determination and laser-induced fluorescence (LIF) for determination of nitric oxide concentration and vibrational temperature were also used. A general conclusion from these measurements was that additional nonintrusive measurements were required. Other measurements identified for these additional nonintrusive techniques were static density and temperature.

At the request of Wright Laboratory, the Calspan/AEDC electron beam fluorescence (EBF) technique was used to measure nitrogen density, nitrogen vibrational temperature, and the arrival time of the helium component of the driver gas. Determination of helium arrival time was needed to help define the usable flow duration. This paper describes the Calspan EBF measurement system, data reduction methods, and the results of the measurements which were performed under Task VI of the program, "Electron Beam Density Measurement in Hypersonic Flow." An analysis of these results are to be reported by Boeing (Ref.4).

The EBF technique uses a narrow beam of high energy (50 keV) electrons to ionize and excite all species of gas atoms and molecules within the path of the beam. As the gas atoms and molecules lose the energy gained from their collisions with the beam electrons, they emit radiation which is characteristic of their particular species. From the intensity and spectral distribution of the fluorescence, species concentration and temperature(s) can be determined, respectively. An overview of the EBF technique is given in Ref. 5.

Molecular nitrogen (N_2) is directly excited by electron impact to the $N_2^+ B\,^2\Sigma_u^+$ electronic state:

$$N_2\,X\,^1\Sigma_g^+(v') + e^- \rightarrow N_2^+\,B\,^2\Sigma_u^+(v) + 2e^-$$

from which spontaneous radiation occurs by

$$N_2^+\,B\,^2\Sigma_u^+(v) \rightarrow N_2^+\,X\,^2\Sigma_g^+(v'') + h\nu(F.N.)(v,v'')$$

where v, v', and v" denote different vibrational levels, X are ground electronic states, and hν (F.N.) denotes radiation from the N_2^+ First Negative System.

The collisional de-excitation (quenching) process deactivates excited state molecules before spontaneous emission can occur; its process is:

$$N_2^+\,B\,^2\Sigma_u^+(v) + N_2\,X\,^1\Sigma_g^+(v') \rightarrow N_2^+(\alpha) + N_2(\beta)$$

in which the final states α and β are unknown. As the number density of the gas increases, this effect becomes more pronounced.

*The research reported herein was performed by the Arnold Engineering Development Center (AEDC), Air Force Systems Command. Work and analysis for this research were done by personnel of Calspan Corporation/AEDC Operations, operating contractor for the AEDC aerospace flight dynamics facilities. Further reproduction is authorized to satisfy needs of the U. S. Government.

In general, observation of an electron beam in a gas with a detection system of efficiency $s(\lambda)$ and solid angle w results in a detector photon rate of

$$S = (\omega/4\pi)s(\lambda)(I/e)\sigma_{gi} n_g L A_{ij}\tau_i/(1 + k_i\tau_i n_g) \quad (1)$$

where I is the beam current, e the electronic charge, σ_{gi} the excitation cross section for the ground state level g to i transition, n_g the ground state number density, L the observed length of beam, A_{ij} the Einstein spontaneous transition probability for the i to j transition, τ_i the radiative lifetime of state i, and k_i the quenching rate constant for level i. The photon rate is directly proportional to the beam current and the ground state number density, but modified by the quenching term in the denominator, whose magnitude depends on the ground state number density. Rather than assigning values to each of these parameters, density calibrations are usually accomplished by using the detection system to measure the photon rate in a gas of known density, while keeping the same optical configuration, transition, etc., for the calibration and test.

The excitation and emission of nitrogen's N_2^+ First Negative System bands are modeled in AEDC's EBFN2 computer program. Results from spectral band measurements are compared to program predictions to obtain rotational or vibrational temperatures. The fluorescent intensity distribution within a rotational band is a function of rotational temperature. The relative fluorescent intensities of two vibrational bands whose upper vibrational levels are different is a function of the vibrational temperature.

Small angle scattering collisions between primary electrons and gas molecules result in gradual spreading of the beam as it traverses the gas. The magnitude of beam spreading is primarily a function of the gas species, the beam energy, the density of the gas, and the distance from the exit orifice. Beam spreading equations (Ref. 6) were invoked for the B30HST setup and conditions; for a 50-keV beam a maximum beam spread of 8 mm at the observation volume was expected. Fields of view of the optical detection systems were designed to encompass this beam width and more.

THE BOEING 30-INCH HYPERSONIC SHOCK TUNNEL (B30HST)

Principal elements of the B30HST are presented in Fig. 1.† It consists of a 160-in.-long, 3-in.-diam combustion driver, a 299-in.-long, 3-in.-diam driven tube, a 175-in.-long, 30-in. exit diameter contoured nozzle, a 40-in.-diam open jet test section, and a vacuum dump tank. The driver is a combustible mixture of nominally 75 percent helium (He), 16.7 percent hydrogen (H_2), and 8.3 percent oxygen (O_2); this mixture is ignited by the simultaneous firing of 21 spark plugs. At a time slightly after peak pressure in the driver, a double diaphragm assembly which separates the driver and driven sections is ruptured by means of an electrical discharge in the argon gas between the two diaphragms. After release of the driver gas, an incident shock wave is formed which travels down the air-filled driven tube and reflects off the nozzle entrance to create the tunnel reservoir conditions. A Mylar® diaphragm which separates the air in the driven tube from the evacuated nozzle, test section, and dump tank is easily ruptured to allow the flow to begin. The nozzle was designed for nominal operation at Mach 16 and a range of operational Mach numbers from 8.5 to 20; for this program a 0.601-in.-diam throat insert was selected to provide a Mach 10 flow in the test section.

A program operational test point was chosen having the following characteristics: stagnation conditions of 5,130 psia pressure (measured) and 6,490 K temperature (calculated from driven tube incident shock speed measurements), free-stream static pressure of 0.034 psia (measured) and 450 K temperature (calculated), free-stream density of 75×10^{-6} lbm/ft^3 (3×10^{16} molecules/cm^3), and a 6.5-in.-thick boundary layer at the exit. The exit plane species mole fractions were calculated to be 0.698 N_2, 0.147 O_2, 0.065 NO (nitric oxide), 0.090 O, 5×10^{-10} N, and 8×10^{-8} NO^+ and e^- (free electrons). The mole fraction of Ar (argon) was not modeled.

Numerous pressure transducers are located along the driver and driven tubes, the throat region, and the nozzle, and are used for evaluation of tunnel performance, nozzle flow-field characteristics and

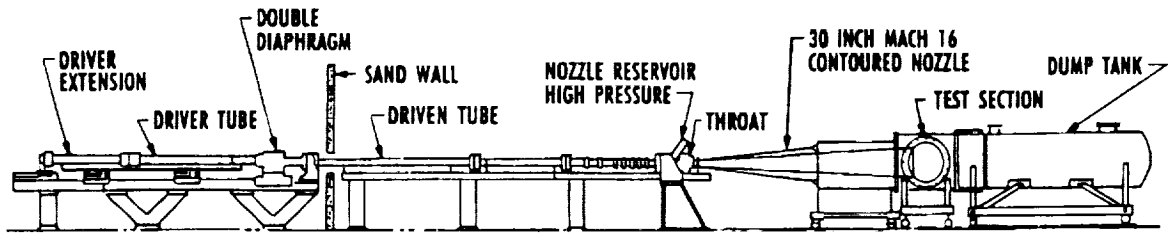

Fig. 1. Boeing 30-in. hypersonic shock tunnel.

† Figures 1–31 are cited in the text.

test section conditions. The signal from a transducer located one inch upstream of the nozzle throat is used to provide a trigger pulse for critically timed events occurring in the test section. To monitor the test section pitot pressure, a two-transducer probe was positioned at the nozzle exit plane such that no interference with the electron beam would occur.

Forty transient data recorders (TDRs) are used for the acquisition of pressure transducer and diagnostic instrumentation outputs at sample rates of up to 500 kHz per channel. For time correlation during a run, all the TDR channels are triggered simultaneously. Data are stored on the TDRs until they are transferred to a PDP-11 hard disk. The data system is capable of manipulating and reducing raw data to standard engineering units. A moving average routine can be applied to the data to filter out any high frequency noise components. Any test specific data reduction routines, such as heat transfer calculations, can readily be included in the system. Reduced parameters can be printed or plotted on a laser printer. Files of raw and reduced data are stored on magnetic tape.

ELECTRON GUN

The AEDC electron gun system was manufactured by Kimball Physics, Inc. The model EMG-22B electron gun has an accelerating potential variable up to 50 kV and delivers up to 10-mA current. It is capable of being modulated at pulse rates from 10 Hz to 10 kHz with pulse widths from 1 to 20 μsec. The gun section, which must be maintained at a pressure of less than 0.1 mtorr, is pumped by a 56-ℓ/sec turbomolecular pump and has deflection and focusing coils that allow the beam to be precisely directed through a 1.0-mm-diam orifice. The base pressure is 1×10^{-7} torr. The original thin-walled copper orifice plate was replaced by a 4.8-mm-thick copper plate having a 1.0-mm-diam orifice, allowing a greater pressure differential and permitting operation in chamber pressures up to about 10 mtorr. The small, retractable, internal Faraday cup was removed from its position near the back side of the orifice. To enable evaluation of the gun performance, the orifice plate was electrically insulated and a lead was attached between it and the former cup's electrical feedthrough to allow external measurement of any orifice plate current. Orifice currents of less than 1 μA can be detected. A pneumatic gate valve is located near the back side of the orifice. After passing through the orifice, another set of deflection and focusing coils provides a steerable beam diameter of 1 to 2 mm at a distance of approximately 0.6 m. A 30-ft-long cable assembly connects the gun with the power supply.

The electron gun installation is illustrated in Fig. 2. An additional orifice and pumping section was required to maintain the gun at an acceptably low pressure (2 torr) during the flow duration of the B30HST. Stainless steel pipe of 2.0-in. inside diameter was used to construct this section. The water-cooled copper orifice plate of this differential pumping system was 2.9 mm thick, had a 2.0-mm-diam orifice, and was located 34 in. from the first orifice and 8 in. above the nozzle centerline. Electrical insulation of the orifice was necessary to enable measurement of orifice plate current. This was accomplished by using a micarta flange and other insulating components between the gate valve and orifice assembly. All the gun system parts within the test section were designed to prevent significant misalignment of the electron beam as the impact of the run occurred. A 50-ℓ/sec turbomolecular pump located outside the test cell pumped this section. To protect the gun and pumping system from the post-flow test section high pressure, an electro-pneumatic gate valve was positioned 4 in. above the second orifice. Immediately following each run, the operator manually closed this valve, closing the system in 1 sec, and turned off the power to the electron gun. A sharp-edged aluminum flow fairing was affixed to the pipe section between the gate valve and orifice to reduce the chance of tunnel blockage and minimize disturbance of the beam alignment by dynamic flow-field loads. To reduce flow distortions and pressure at the orifice exit, a 6.0-in.-wide, 5.2- in.-long, sharp-

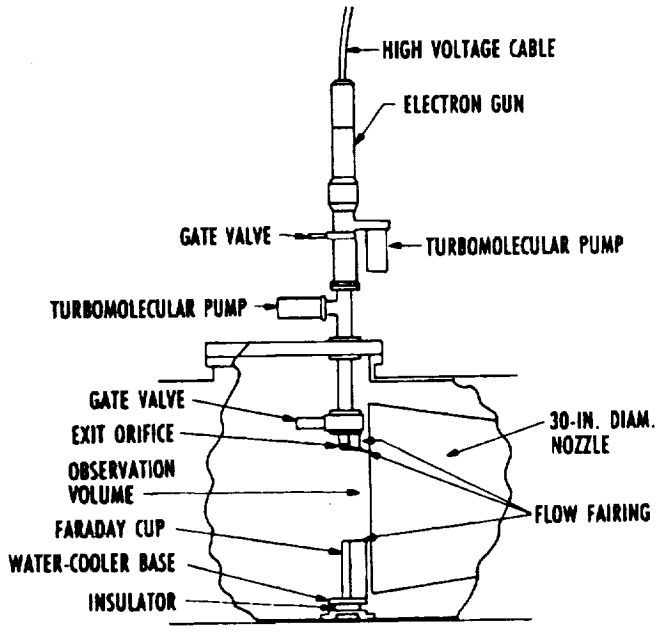

Fig. 2. Side view of B30HST with electron gun installation.

edged flat plate was bolted to the bottom of the orifice assembly.

Electron beam current was collected by a 2.25-in. inside diameter, 9.5-in.-long, copper Faraday cup whose entrance was 7 in. below nozzle centerline. The cup was attached to a water-cooled copper base which was firmly bolted to and insulated from the bottom of the test section. A flow fairing was placed upstream of the cup to reduce interactions with the flow field.

OPTICAL INSTRUMENTATION

A plan view of the optical instrumentation layout is given in Fig. 3. Molecular nitrogen number density was measured by two identical AEDC systems. Fused silica lenses were used in both assemblies to reduce transmission losses. The north side system was tilted at a 10-deg angle, to observe the nozzle centerline downward through a window. This window was located directly above the window which accommodated the Boeing photomultiplier tube (PMT) detector system. Fluorescence at 391 nm was collected by a 7.38-in. focal length, 3.0-in.-diam lens at an object distance of 26.75 in. Before coming to a focus, the light was collimated to a 0.55-in.-diam by a −1.92-in.-focal length, 1.0-in.-diam, plano-concave lens. The collimated light passed through an interference filter before being focused onto the aperture of the PMT by a 3.83-in. focal length, 1.0-in.-diam plano-convex lens. Vignetting was minimized by reducing the separation of the two small lenses as much as possible. These optics projected the PMT aperture

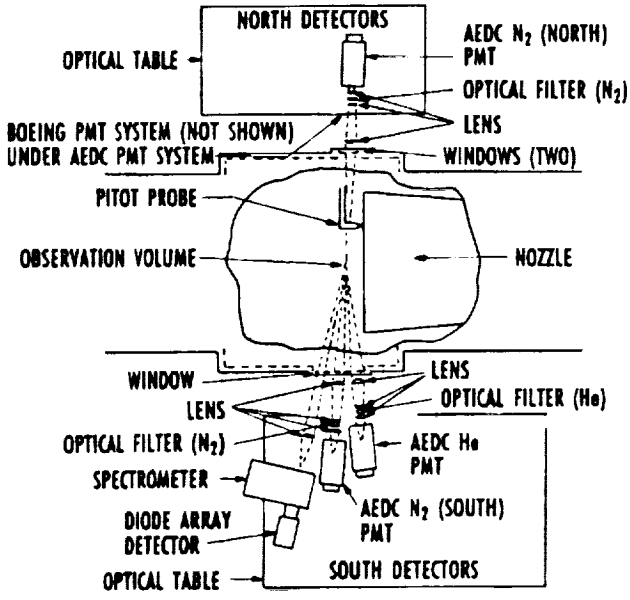

Fig. 3. Plan view of B30HST and Boeing/AEDC optical diagnostics installation.

dimensions onto the nozzle centerline by a magnification factor of 1.31, giving a resultant field of view of 30 mm horizontal and 10 mm vertical. Collection of fluorescence from the total width of the beam was assured by this arrangement. The south side PMT system was centrally located and was level. The north and south side AEDC nitrogen PMT systems were designated AEDC N_2 (North) and AEDC N_2 (South), respectively, in Fig. 3 and in following figures.Each 1.0-in.-diam nitrogen optical interference filter has a 39-percent transmission at the peak wavelength of 390.8 nm, a full-width half-maximum (FWHM) bandpass of 3.85 nm, and an optical density of four for blocking from 200 to 950 nm.

Similar optics were assembled for the AEDC helium PMT detector system, located adjacent to the south side nitrogen system. A 5.88-in. focal length, 3.0-in.-diam fused silica lens collected the light. A glass plano-convex lens of −1.96-in. focal length and 1.6-in. diam was placed before the focus to collimate the light to a diameter of 0.8 in., thus accommodating the 1.0-in.-diam helium interference filter. A glass plano-concave lens of 4.0-in. focal length and 1.25-in. diam focused the collimated light onto the PMT aperture, which was rotated 90 deg with respect to both nitrogen system apertures, allowing collection of light from a longer length of beam. This optical system provided a magnification factor of 1.74 of the PMT aperture dimensions onto the nozzle centerline, for a resultant field of view of 13 mm horizontal and 40 mm vertical. The helium optical interference filter had 50-percent transmission at the peak wavelength of 501.6 nm, a FWHM of 0.84 nm, and the same blocking characteristics as the nitrogen filters.

For noise reduction, the RCA C31034A PMTs were contained within thermoelectric coolers held at a temperature of −20°C. These PMTs feature high quantum efficiency and sensitivity, spectral response from 200 to 930 nm, extremely low dark noise, and fast time response characteristics. Each PMT required a separate high-voltage power supply.

An Acton Research Corporation SpectraPro-275 spectrometer coupled with a linear diode array detector was set up to measure nitrogen vibrational temperature. The spectrometer has a 0.275-m focal length, an f/3.8 aperture ratio, adjustable slits, and a 25-mm-wide focal plane. The three gratings which were mounted on the triple indexable turret had the following characteristics: 1,200 lines/mm holographic, 2,400 lines/mm holographic, and 3,600 lines/mm blazed at 240 nm. The 3,600 lines/mm grating was not used because its efficiency at 425 nm wavelength was determined at AEDC to be too low. A reciprocal linear dispersion of 3.0 nm/mm occurs for the 1,200 lines/mm grating.

Dispersed spectra were detected and processed by an Optical Spectrometric Multichannel Analyzer (OSMA) system. The detector was a Princeton Instruments, Inc. proximity focused MCP image intensified detector, model IRY-1024 S/RB. It is a gatable detector with extended coverage in the UV and red wavelength regions. There are 1,000 active 25-μm-wide by 2.5-mm-high diodes. The total array width of 25 mm matches the spectrometer's focal plane width. The detector yields 0.13 counts/photon at 425 nm wavelength, and its gain is not adjustable. Allowable gate widths range from 200 μsec to 6 msec. Control of the detector was by means of Princeton Instruments model PG-10 Pulse Generator and model ST-100 Detector Controller. Tap water was circulated through the detector's thermoelectric cooler to reduce the temperature to −20°C, thereby reducing the noise level. A desktop computer running Princeton Instruments software was used for data recording and processing.

A plano-convex fused silica lens collected the fluorescence and focused it onto the spectrometer slit. This 3.0-in.-diam lens had a 5.91-in. focal length at the nitrogen First Negative System (0,1) band's wavelength of 427 nm. The object and image distances were 39.0 and 7.0 in., resulting in a projection of the slit dimensions onto the observation volume with a magnification of 5.6.

BOXCAR SYSTEM

Figure 4 shows a simplified block diagram of a typical boxcar integrator channel which was used for the basic data acquisition subsystem. The input to the boxcar integrator was the signal from a single PMT, and its output was passed to a single TDR channel. The basic function of the integrator channel was to sample the PMT signal and hold it for output to the TDR. A single sample was obtained for each trigger of the boxcar channel.

The signals from the PMTs were anode currents whose amplitudes were representative of the signals observed from the sample volume. These currents were of sufficient magnitude that preconditioning was not required before input to the boxcar integrator. Because no external amplifier was used, sensitivity was controlled by adjustments in PMT high voltage and in the integrator time constant and gain. Settings were made according to the anticipated PMT signal levels and were manually recorded for use in posttest calibration and data reduction.

Four boxcar channels were required for the four PMT inputs. A fifth channel was used to obtain a second, time-delayed sample of the He PMT signal during a given data cycle. Dual sampling of the He PMT signal was possible because each boxcar channel gate could be independently triggered and optionally delayed with respect to the trigger. The delay capability was also used to obtain the gate for the AEDC N_2(North) PMT signal, coincident with the second He PMT signal sample. Gating circuits and timing diagrams are shown in Figures 5a and 5b.

During each data cycle the integrator circuit sampled the PMT output. Concurrently the integrator sample/hold circuit provided data read during the previous cycle to the TDR. Thus, while the system was recording a previously obtained sample, a new data sample was being generated.

The system of five boxcar channels was paced by the internal oscillator of the first channel [AEDC

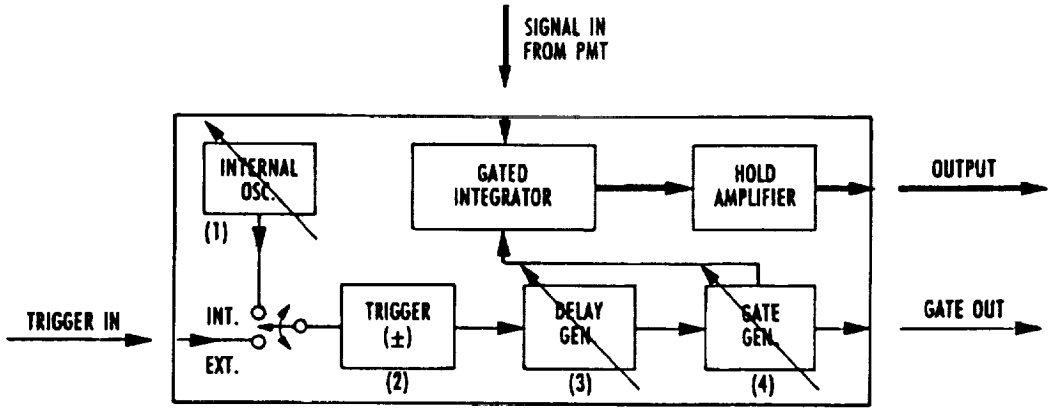

Fig. 4. Simplified block diagram for single gated integrator channel.

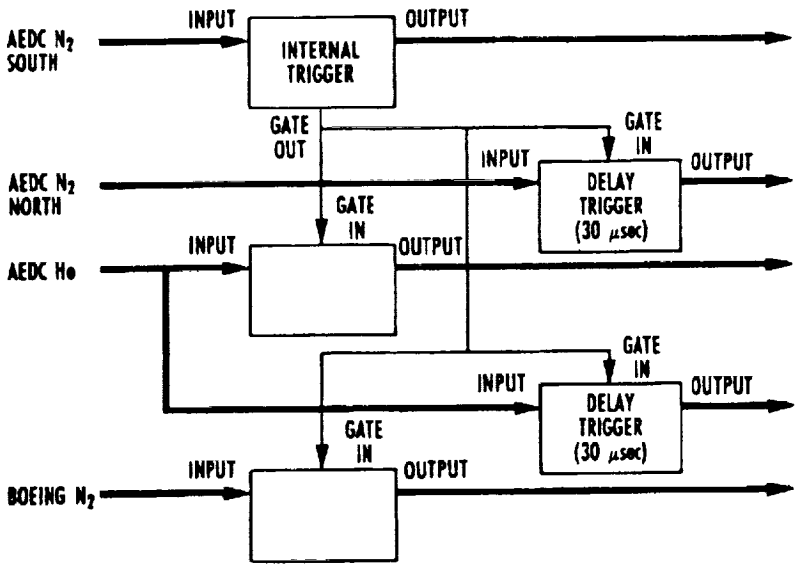

a. Interconnection of integrators

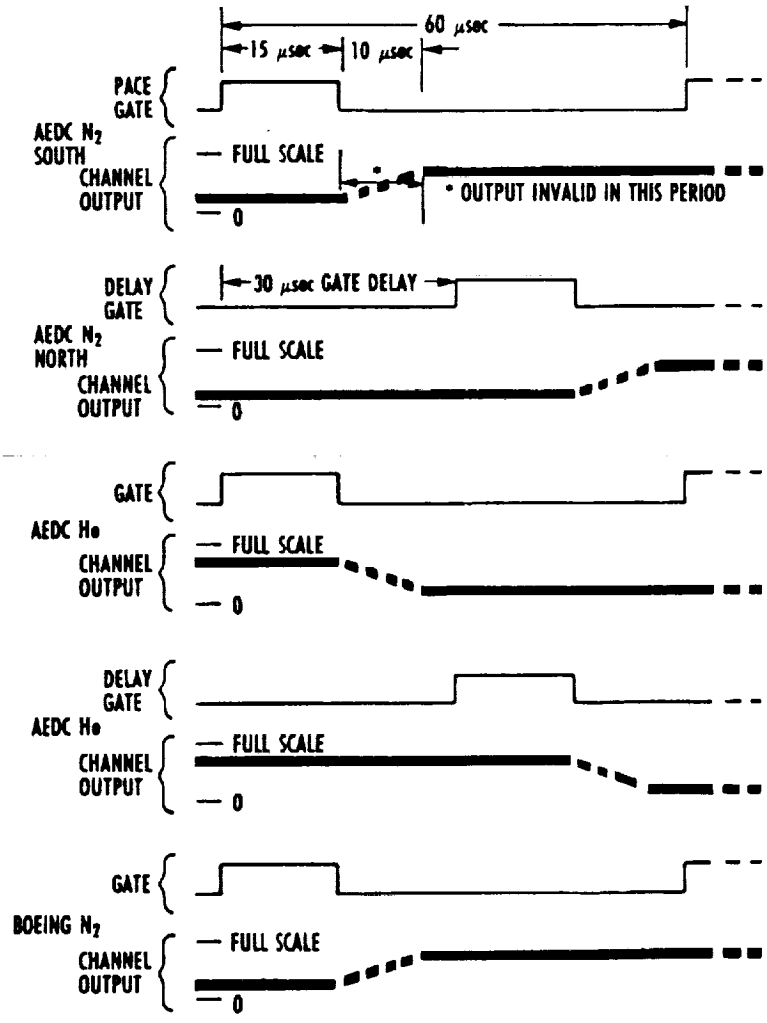

b. Timing diagram

Fig. 5. Block diagram and timing diagram for PMT gated integrators.

N_2(South)] running at near-maximum rate (16.7 kHz). The leading edge of the pace integrator gate simultaneously triggered the other four channels. The integrator gates for the He and Boeing N_2 channels occurred simultaneously with that of the pace channel. The integrator gates for the AEDC N_2(North) and He^{del} channels were delayed by 30 μsec. All gate durations were set at 15 μsec. Following each integrator gate, a period of 10 μsec was required to perform the integration and sample/hold operations, during which the output was invalid (Fig. 5b). The data cycle time was set at 60 μsec. This yielded a 16.7-kHz sampling rate for all channels. Because of dual sampling, an effective rate of 33.3 kHz was achieved for the helium PMT. Each integrator channel output was sampled several times during each data cycle as a result of the significantly higher sampling rate (500 kHz) of the TDR data recording system.

DATA

RADIATIVE SPECIES

Spectra obtained by the spectrometer/array detector system during 14 of the runs listed in Table 1 are shown in Figs. 6-19. A variety of atomic lines and molecular bands were recorded and identified; they are listed by occurrence in Table 1 and by wavelength in Table 2, and their time history is plotted in Fig. 20. Data were acquired using three combinations of spectrometer gratings and central wavelength settings. The spectra include spurious positive and negative pulses and flat regions which are artifacts of the detector operation and should be ignored.

Wavelength scales were based on calibrations obtained from both Hg lamp spectra and other spectral features that were subsequently identified. Numbers on the ordinates correspond to detector output counts. Intensity scales, expressed in detector counts, were selected for optimum viewing.

Table 1. Spectrometer/Array Detector Results

RUN	BEAM	TRIG	EXP	GRAT	WAVE	SPECTRA
8001						BOMB SHOT; DETECTOR NOT IN SERVICE.
8002	ON	+0.3	2.0	2400	425	Cr I - THREE LINES. Fe I - ABOUT EIGHT LINES.
8003	OFF	0.0	2.0	1200	413	Cr I. Al I - TWO LINES. Mn I. MANY Fe LINES.
8004	OFF	0.0	1.0	1200	413	LIKE RUN 8003.
8005	ON	NO	RECORD	1200	413	SOME SATURATION; SOME DIFFERENCE FROM RUNS 8003 AND 8004.
8006	ON	0.0	1.0	1200	413	NO SPECTRUM; MISTRIGGERED.
8007	OFF	−0.5	1.0	1200	413	LIKE RUNS 8003 AND 8004 BUT VERY WEAK.
8008	OFF	+0.1	0.5	1200	413	LIKE RUN 8007.
8009	ON	+0.3	0.5	1200	413	STRONG N_2^+ FIRST NEG. (0,0) AND (0,1) BANDS.
8010	ON	0.0	1.0	2400	425	N_2^+ (0,0) AND (0,2) OVERLAID BY Cr I AND Fe I.
8011	ON	−0.5	0.5	2400	500	NO He I 501.6 NM LINE. CU 510.6 NM LINE. NITRIC OXIDE (0,2) BANDS.
8012	OFF	+0.2	1.0	2400	425	LIKE RUN 8002.
8013	ON	0.0	1.0	2400	425	LIKE RUN 8010.
8014	ON	0.0	0.5	2400	500	Cu 510.6 NM.
8015	ON	+4.0	1.0	2400	500	STRONG He I. AIO GREEN (0,1), (1,2), AND TAIL OF DELTA V = 0 BANDS. NO NITRIC OXIDE BANDS.
8016	ON	0.0?	1.0	2400	500	STRONG Cu I. MANY Fe I LINES IN ORDER II. NO He I. NO NITRIC OXIDE BANDS.
						TRIG = TRIGGER TIME RELATIVE TO PEAK PRESSURE AT NOZZLE EXIT, IN MSEC. EXP = EXPOSURE TIME IN MSEC. GRAT = GRATING LINES/MM (2400 IS HIGH RESOLUTION). WAVE = SPECTROMETER CENTER WAVELENGTH, NM.

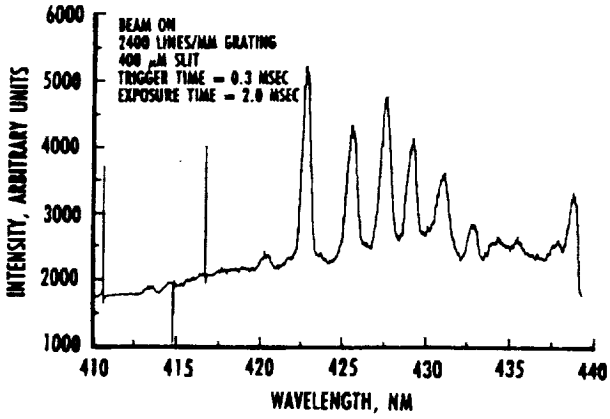

Fig. 6. Spectrometer/array detector spectrum for Run 8002.

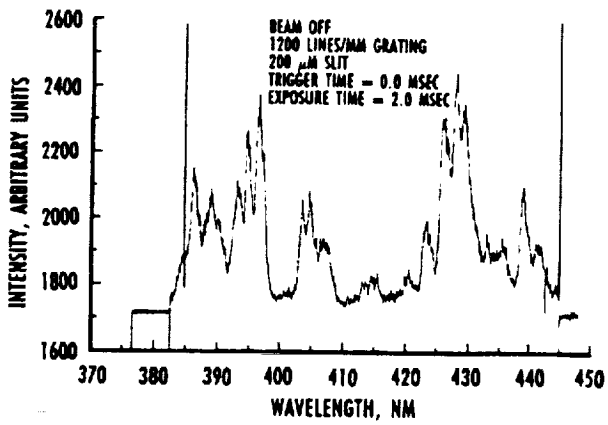

Fig. 7. Spectrometer/array detector spectrum for Run 8003.

The higher resolution of the 2,400 lines/mm grating with respect to the 1,200 lines/mm grating is evident, for example, upon comparison of the three chromium lines in Runs 8002 and 8003 (Figs. 6 and 7). To reduce scattered light, portions of the test section were spray painted flat black. Residual airborne particles from the paint apparently caused a large increase in scattered light, resulting in saturation of the spectra in Run 8005 (Fig. 9). Later, the blackening seemed to be effective, as indicated by the reduced background spectra of Runs 8007 and 8008 (Figs. 10 and 11). The effectiveness of the blackening is also indicated in Run 8009 (Fig. 12) by the strength of the electron beam-excited (0,0), (1,2), and (0,1) nitrogen First Negative System bands with respect to the background metal lines. Inexplicably,

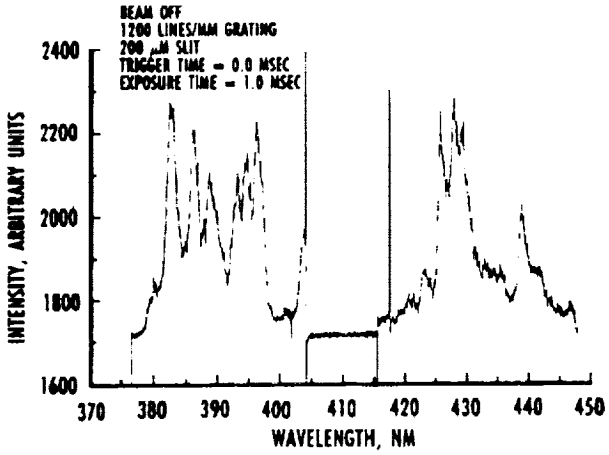

Fig. 8. Spectrometer/array detector spectrum for Run 8004.

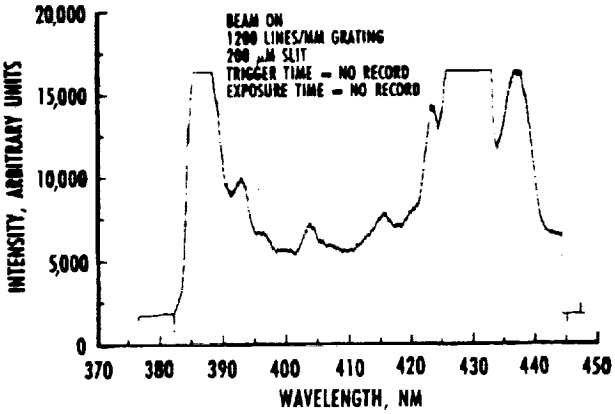

Fig. 9. Spectrometer/array detector spectrum for Run 8005.

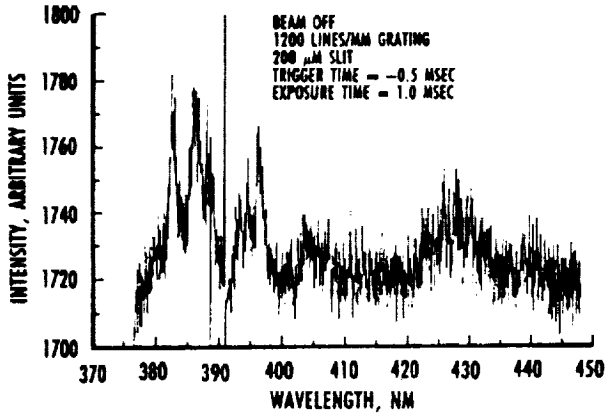

Fig. 10. Spectrometer/array detector spectrum for Run 8007.

spectra from the remaining runs with the center wavelength set at 425 nm were again dominated by the metal lines. For Runs 8010 and 8013 (Figs. 13 and 16), the (1,2) and (0,1) bands, which appear at

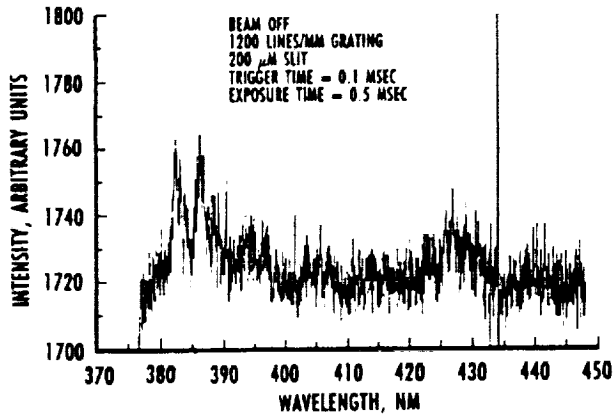

Fig. 11. Spectrometer/array detector spectrum for Run 8008.

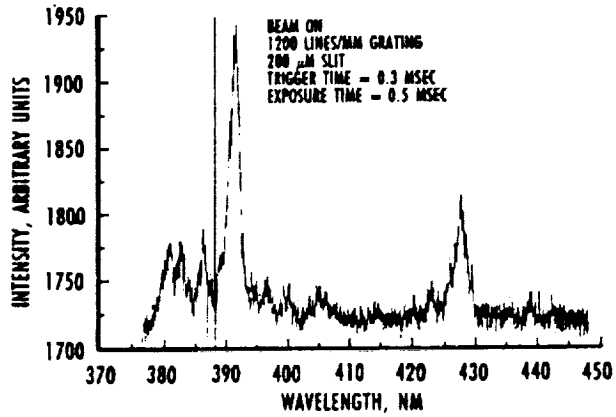

Fig. 12. Spectrometer/array detector spectrum for Run 8009.

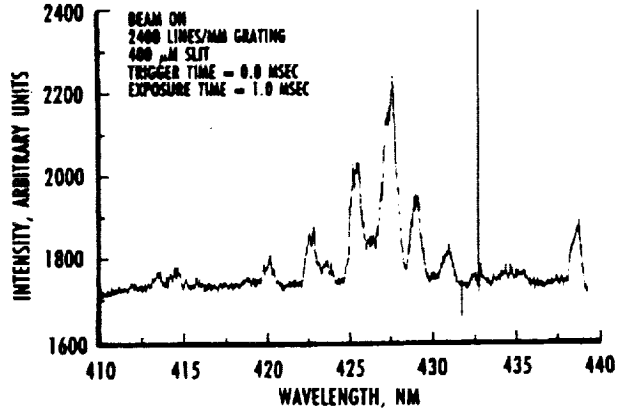

Fig. 13. Spectrometer/array detector spectrum for Run 8010.

423 nm and 427 nm, respectively, are weak with respect to the strong metal lines. Electron beam-excited NO bands were recorded in the early part of Run 8011 (Fig. 14), and AlO bands were recorded in the latter part of Run 8015 (Fig. 18).

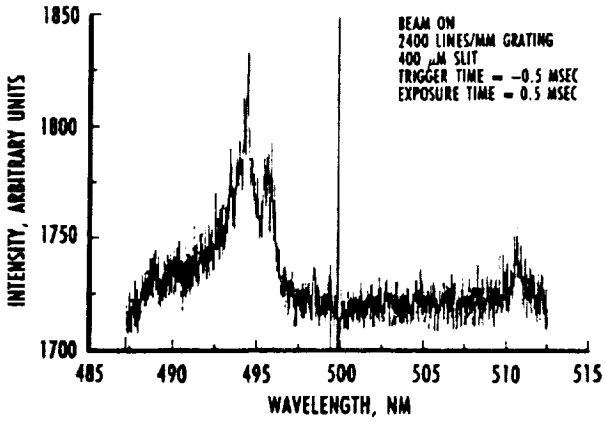

Fig. 14. Spectrometer/array detector spectrum for Run 8011.

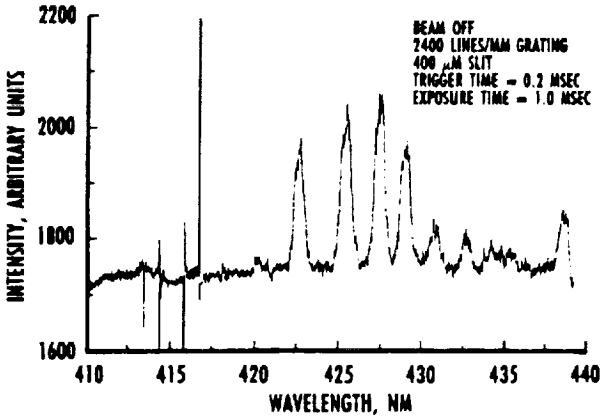

Fig. 15. Spectrometer/array detector spectrum for Run 8012.

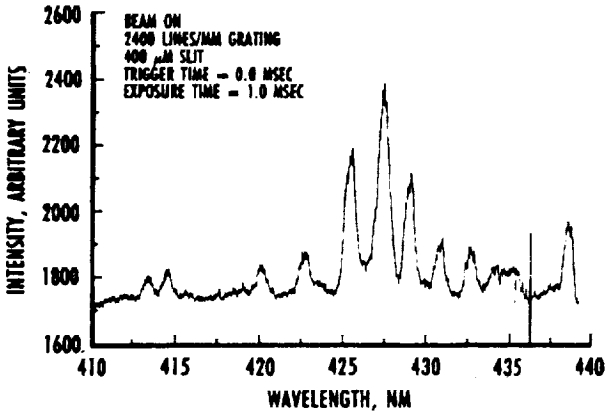

Fig. 16. Spectrometer/array detector spectrum for Run 8013.

HELIUM ARRIVAL TIME

The spectrometer/array detector system was set to record the helium 501.6-nm line in four of the last six runs. With respect to the peak pressure at the nozzle exit, the trigger time of the detector was shifted as shown in Table 1. These data (see Fig. 20), in conjuction with other evidence, indicate that the chemically pure test time of the B30HST lies between 1.0 and 2.4 msec.

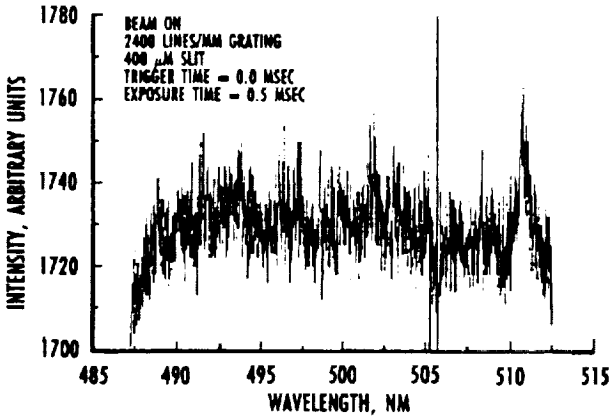

Fig. 17. Spectrometer/array detector spectrum for Run 8014.

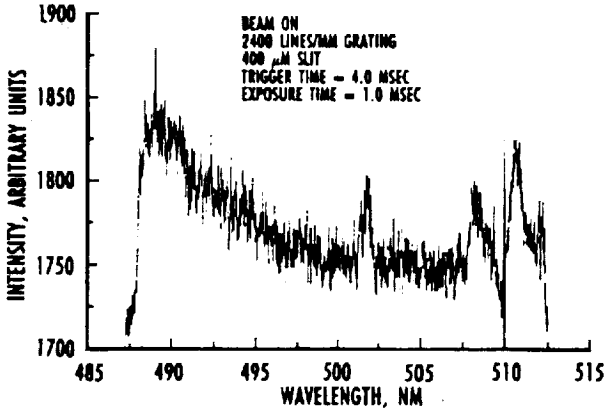

Fig. 18. Spectrometer/array detector spectrum for Run 8015.

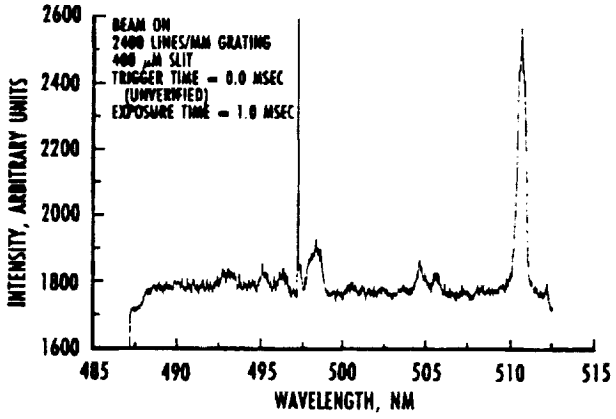

Fig. 19. Spectrometer/array detector spectrum for Run 8016.

Table 2. Spectral Features

WAVELENGTH, NM	SPECIES	WAVELENGTH, NM	SPECIES
382.6	Fe I 382.588	427.5	Cr I 427.480
386.0	Fe I 385.991	427.8	N_2^+ FIRST NEG. (0,1) BH
388.6	Fe I 388.628	429.0	Cr I 428.972
391.4	N_2^+ FIRST NEG. (0,0) BH	430.8	Fe I 430.791
392.8 393.0	Fe I 392.792 393.030	432.6	Fe I 432.576
		435.3	Fe I 435.274
394.4	Al I 394.403	437.6	Fe I 437.593
396.2	Al I 396.153	438.4	Fe I 438.355
403.1	Mn I 403.075	494.2 495.7	NO GAMMA (0,2) BH, ORDER II
404.6	Fe I 404.581	501.6	He I 501.567
406.4	Fe I 406.360	507.9	AlO GREEN (0,1) BH
420.2	Fe I 420.203	510.2	AlO GREEN (1,2) BH
422.7	Fe I 422.743	510.6	CU I 510.554
423.7	N_2^+ FIRST NEG. (1,2) BH		
425.4	Cr I 425.435		

BH = BANDHEAD

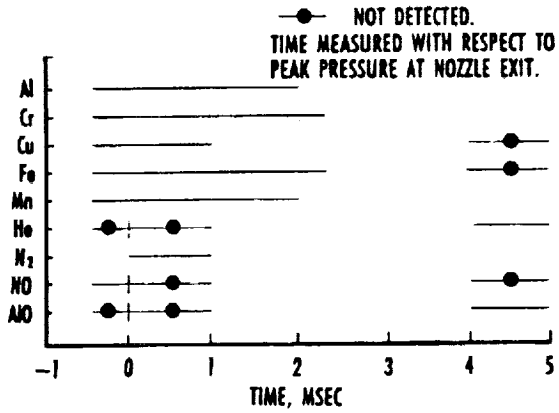

Fig. 20. B30HST species time history.

DENSITY

Before each run, the PMT detection systems for the nitrogen number density measurements were calibrated using a gas of known density. This was accomplished by evacuating the test chamber, readmitting air to a measured level of temperature and pressure, and measuring the fluorescence collected by the actual PMT optical systems, signal conditioning, and data recording equipment. The detector collection optics were configured to ensure complete collection of the electron beam width. The electron beam current was manually recorded. Recorded fluorescent signals were normalized with the Faraday cup current values. Calibrations at pressures greater than 800 mtorr at 300 K (2.6×10^{16} cm^{-3} or 77×10^{-6} lbm/ft^3) could not be obtained because of poor gun performance at higher pressure levels.

For each calibration pressure, the density calibration factor A_{N_2} is defined by

$$A_{N_2} = n_{N_2}^{cal,q}/(S^{cal}/i^{cal}), \quad (2)$$

where S^{cal} is the detector's calibration signal, i^{cal} is the beam current at calibration, and $n_{N_2}^{cal,q}$ is a modified nitrogen calibration density $n_{N_2}^{cal}$ defined by

$$n_{N_2}^{cal,q} = n_{N_2}^{cal}/(1 + n_{Air}^{cal} k\tau), \quad (3)$$

where the quenching constant $k\tau = 1.6 \times 10^{-17}$ cm^3/molecule (obtained from prior AEDC studies). The quenched calibration signal is, therefore, coupled with an equivalently reduced value of the nitrogen calibration density. Application of the quenching factor requires the product of $k\tau$ and the air density, not the nitrogen density. In air, it is assumed that the oxygen and nitrogen quenching constants are equal.

For a given test, the modified nitrogen test density is defined by

$$n_{N_2}^{test,q} = A_{N_2} S^{test}/i^{test}, \quad (4)$$

and the actual nitrogen number density is

$$n_{N_2}^{test} = n_{N_2}^{test,q} \Big/ \left[1 - \left(n_{N_2}^{test,q} / M_{N_2}^{test} \right) k\tau \right], \qquad (5)$$

where $M_{N_2}^{test}$ is the nitrogen mole fraction in the test gas.

All density data were corrected for the difference in vibrational temperature between the calibration and test conditions. The fraction of nitrogen molecules in the lowest vibrational level (v = 0), which is the level of the measured First Negative System (0,0) band, decreases with increasing vibrational temperature as higher vibrational levels (v = 1, 2, ...) become more populated. This fraction is given by:

$$n(v = 0)/n = 1 - \exp(-3390/T_v), \qquad (6)$$

where T_v is the vibrational temperature. The measured value of T_v, 1,240 K (see next section), yields a fraction of 0.935. Therefore, to correct for the difference in vibrational temperature, the measured densities were divided by this factor.

Reduction of the PMT detector system density data required subtraction of background light. The magnitude of the background light was assumed equal to the magnitude of the light recorded during a run having similar combustion characteristics and with the electron beam off. Data for Run 8010 were reduced using background light from Run 8008. Similarly, background light from Run 8012 was used to reduce the Run 8014 data. Runs 8012 and 8014 were classified as detonations (the diaphragms broke because of high pressure instead of the electrical discharge) as opposed to the preferred combustions, but their stagnation and pitot pressure traces were representative of the desired conditions. It was necessary to use the value of beam current existing just before each run, as the current data obtained during each run were noisy (large harmonics with a prominent superimposed beat structure). Among the causes for this were electrical signals generated by varying capacitance to ground, induced by shock and vibration of the Faraday cup during the run.

No quantitative information was extracted from either of the two south side AEDC PMT detectors. Signals from these detectors were never above background levels. For each run, a strong, spurious burst of signal was detected by both south side PMTs beginning approximately 1 msec before any indication of flow by the pitot probe. These bursts lasted for about 1 msec, ending at nearly the same time that flow was detected. The bursts could have been caused by light originating in the high-temperature stagnation region near the nozzle throat at the driven tube end wall, then reflected by surfaces into the test section. Another possibility was that the south side signal cables were exposed to electrical interference as a result of their particular routing.

Through Run 8012, no useful He PMT data had been acquired. To obtain another time-resolved helium data channel, the AEDC N_2(South) PMT was converted to a helium detector after Run 8012. Neither He PMT detector system ever recorded an identifiable signal above background.

The respective calibration constants for Runs 8010 and 8014 were 2.43 × 10^{14} and 2.23 × 10^{14} molecules/cm^3/(mV/mA) (average of two calibrations for each run). Runs 8010 and 8014 were reduced using, respectively, Runs 8008 and 8012 for the background, and the vibrational temperature correction was applied. These results are presented in Figs. 21 and 22. Theoretical frozen densities shown in the figures were calculated under the assumption of fully frozen flow in the nozzle expansion, while the theoretical equilibrium densities assume full chemical equilibrium during the nozzle expansion. The PMT system results are presented in two ways: (1) using the quenching constant kτ = 0 (no quenching in the flow), and (2) kτ = 1.6 × 10^{-17}cm^3/molecule. For Run 8010 most of the PMT system values using kτ = 1.6 × 10^{-17}cm^3/molecule are greater than the frozen flow values. For Run 8014 more of the PMT system values using kτ = 1.6 × 10^{-17}cm^3/ molecule are less than the frozen flow values. It should be noted that, at these high densities, even a slightly smaller quenching constant would substantially

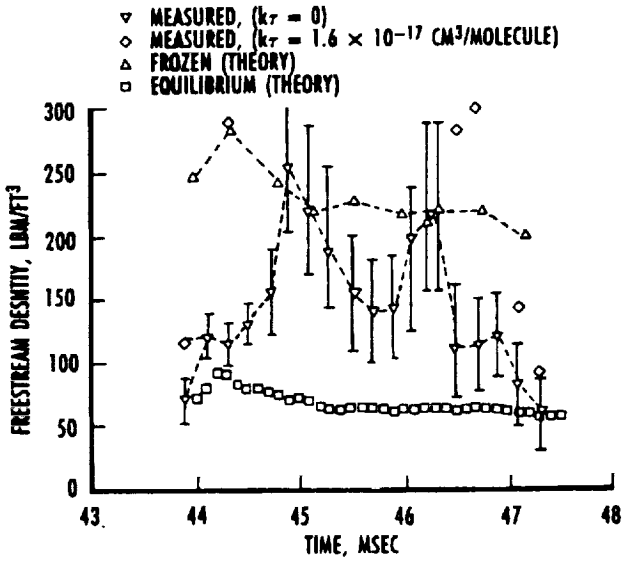

Fig. 21. Measured and theoretical flow densities for Run 8010.

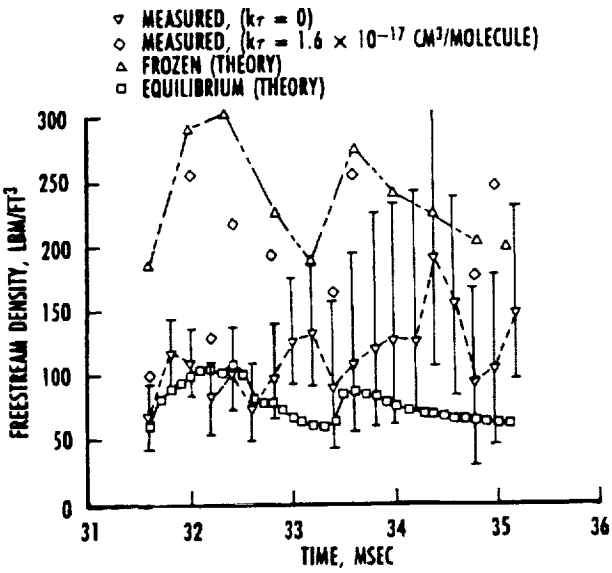

Fig. 22. Measured and theoretical flow densities for Run 8014.

reduce the PMT system values. It is certainly possible that, given the species content (N_2, O_2, NO, O) and higher temperatures of the flow, a quite different value of the quenching constant occurs. Uncertainty bars on the PMT system results derived from variations of background light levels.

Meaningful density results using the AEDC N_2(North) PMT were obtained only for Runs 8010 and 8014. The reduced data for Runs 8013 and 8015 were well above the upper bounds set by theoretical predictions. No PMT system data was obtained for Run 8009 because of misalignment of the AEDC N_2(North) detector.

NITROGEN VIBRATIONAL TEMPERATURE

A vibrational temperature can only be extracted from two spectral bands having different upper vibrational energy levels. It is advantageous to select two bands of close proximity in wavelength. The (0,0) band is the strongest feature of the nitrogen First Negative System, but its accompanying (1,1) band is too weak at low vibrational temperatures. For this application, the optimum pair of bands was (0,1) and (1,2). They appeared in the array detector spectra of Runs 8009, 8010, and 8013 at their wavelengths of 427 nm and 423 nm, respectively.

Figure 23 shows a magnified spectrum obtained during Run 8009. Although the spectrum was recorded with the low-resolution grating, the (1,2) and (0,1) bands were separated sufficiently. The background level was chosen as shown, tails were faired in to the zero level by hand at both ends of each band, and the band areas were measured using a polar planimeter. The ratio of these areas, 6.27, was the ratio of total band intensities. This ratio must be corrected for spectral sensitivity of the spectrometer/array detector system. A spectral sensitivity calibration using a standard tungsten strip lamp determined that the sensitivity at 423.5 nm was 1.8 percent greater than that at 427.8 nm when using the 1,200 lines/mm grating. Accounting for this higher sensitivity, the area ratio became 6.38. Considering possible errors in ascribing the tails and background to the bands, a standard deviation of 0.53 (8.5 percent) was estimated for the area ratio.

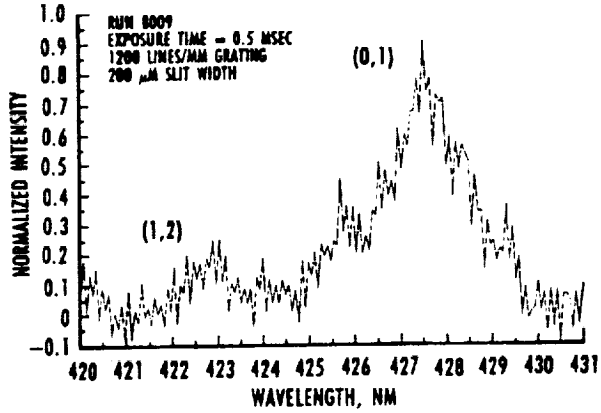

Fig. 23. Nitrogen (0,1) and (1,2) bands for Run 8009.

The 425.4- and 427.5-nm chromium lines occur within the wavelength range of the (0,1) band. The band can be observed convolved with these two lines in the spectra of Runs 8010 and 8013 (Figs. 13 and 16, beam on), when compared with Run 8012 (Fig. 15, beam off). The relative intensities of the three chromium lines remained reasonably constant in Runs 8002, 8003, 8004, and 8012 (Figs 6, 7, 8, and 15). The 429.0-nm chromium line was used as a reference line, since it does not fall within the (0,1) band. After background correction the magnitude of the 429.0-nm line of Run 8012 (Fig. 15, beam off) was adjusted to match the magnitude of that line in Run 8010 (Fig 13. beam on). Results are presented in Fig. 24. The difference in area of the two spectra between 424.8 and 428.4 nm represents the area of the Run 8010 (0,1) band.

To obtain the area of the (1,2) band, a different procedure was necessary because the (1,2) band was convolved with the 422.7-nm iron line. The intensity of the iron line was observed to be independent of the intensities of the chromium lines from run to run. The magnitude of the 422.7-nm line of Run 8012 (Fig 15, beam off) was adjusted to become only slightly smaller than the same line of Run 8010 (Fig. 12, beam on), especially on the low-wavelength

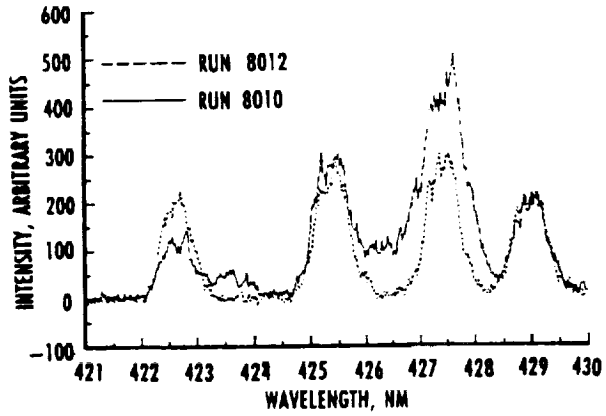

Fig. 24. Matched spectrum for Run 8010 (0,1) band.

side of the line where the weak tail of the R branch of the (1,2) band should be. This result is shown in Fig. 25. The difference in area of the two spectra between 422.0 nm and 424.3 nm represents the area of the Run 8010 (1,2) band.

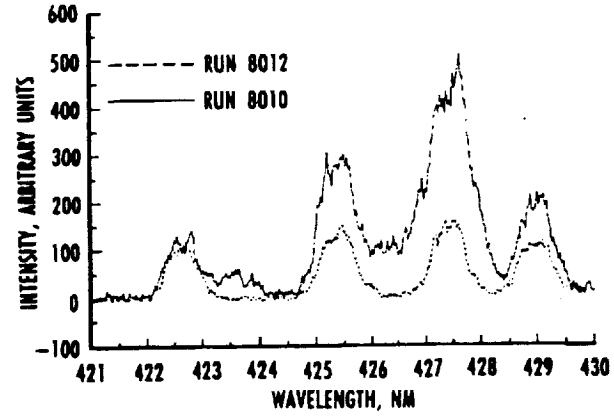

Fig. 25. Matched spectrum for Run 8010 (1,2) band.

The final deconvolved Run 8010 nitrogen band spectrum is presented in Fig. 26. The (0,1) band portion of the spectrum was obtained by subtracting the spectra in Fig. 24. Similarly, the (1,2) band portion is the difference between the Fig. 25 spectra. The two portions were joined at 424.45 nm.

Areas of the (0,1) and (1,2) bands were measured between their respective wavelength limits. The (0,1) to (1,2) area ratio was found to be 5.81 with an estimated standard deviation of 0.63 (10.8 percent), mainly attributed to uncertainty in establishing the relative magnitudes of the 422.7-nm iron line. Based on a tungsten strip lamp calibration, no spectral sensitivity correction was needed when the 2,400 lines/mm grating was used at these wavelengths.

The same matching procedure was carried out for Run 8013 (Fig. 16, beam on) in conjunction with

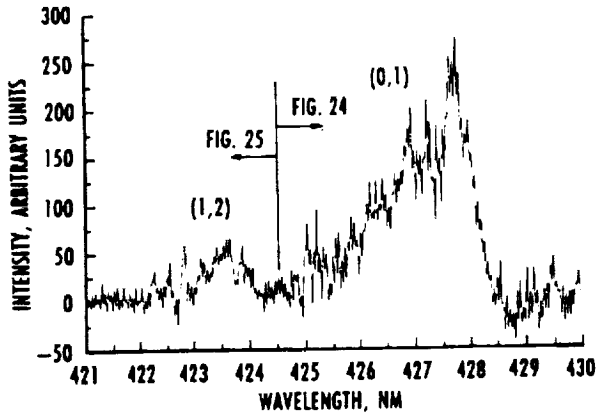

Fig. 26. Nitrogen (0,1) and (1,2) bands for Run 8010.

Run 8012 (Fig. 15, beam off). These results are given in Figs. 27-29. The resultant area ratio was 6.27, with an estimated standard deviation of 0.82 (13.0 percent).

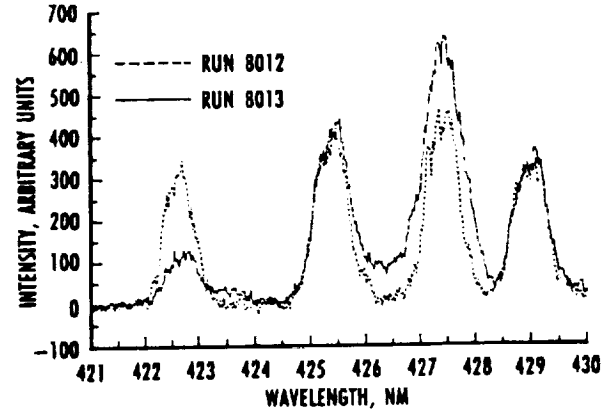

Fig. 27. Matched spectrum for Run 8013 (0,1) band.

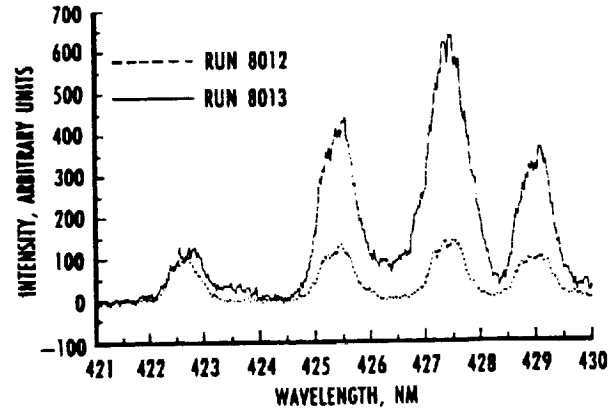

Fig. 28. Matched spectrum for Run 8013 (1,2) band.

Theoretical calculations of electron beam fluorescence for nitrogen are performed by an AEDC computer program designated EBFN2. Although quite comprehensive, the program does not include second-

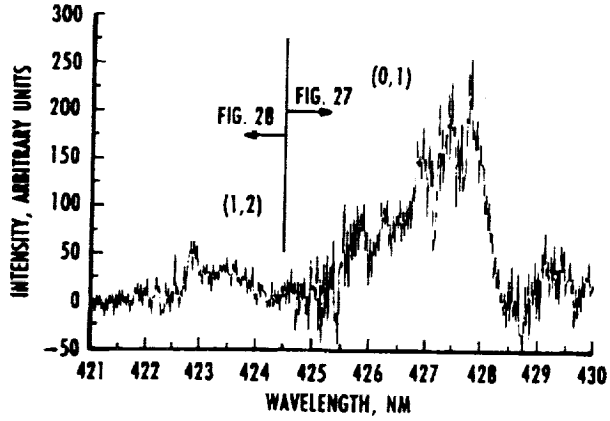

Fig. 29. Nitrogen (0,1) and (1,2) bands for Run 8013.

ary electron effects, collisional and resonant photon excitations, convective and diffusion populating/depopulating mechanisms, and variations in quenching rate with rotational-vibrational level. The program was used to predict the ratio of the (0,1) and (1,2) band intensities as a function of vibrational temperature. The result of the prediction is given in Fig. 30, with the ratios normalized to 1.0 at a vibrational temperature of 300 K. For the reported measurements, the tails of each band were faired in before integration of the areas with the polar planimeter. For comparison with Fig. 30, the experimental area ratios were divided by 8.5, the value of the (0,1) to (1,2) area ratio measured in static conditions in the B30HST at 300 K.

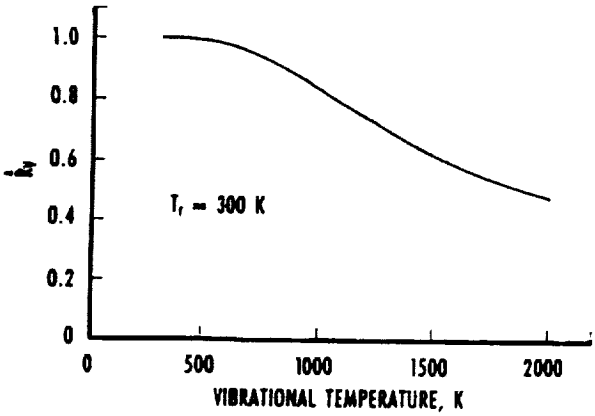

Fig. 30. Normalized intensity ratio of the (0,1) and (1,2) bands as a function of vibrational temperature.

Using the curve in Fig. 30, the measured band area ratios for the three runs converted into vibrational temperatures of 1,180 K, 1,330 K and 1,210 K, giving an average value of 1,240 K. Upon consideration of measurement uncertainty and uncertainties of parameter values used in the calculation by program EBFN2, a standard deviation of 100 K (8.1 percent) was estimated.

NITRIC OXIDE ROTATIONAL TEMPERATURE

A spectrum of the NO Gamma System's (0,2) band was recorded by the spectrometer/array detector system in Run 8011 (Fig. 14). Although both tunnel diaphragms broke prematurely in this run, resulting in unusable flow conditions, it was of interest to determine the NO rotational temperature from the band profile. To determine a free-stream rotational temperature, an AEDC program designated EBFNO was developed for predicting the electron beam excitation and spontaneous emission process. This new computational model assumed that the excitation process was by primary beam electrons and that optical excitation rules applied. Collisional quenching was accounted for in the model, but variation in quenching rate with individual rotational levels was not included. Self-absorption of the electron beam-excited fluorescence was neglected; it is believed that this was a reasonable assumption because of the relatively low population of the third vibrational level of the ground electronic state. It is almost certain that the neglect of the influence of the beam's secondary electrons was not a good assumption, but fiscal limitations prevented development of a more complex model. The spectral relations and parameters in the model were taken from an existing program (LIFNO) developed at AEDC for modeling the laser-induced fluorescence process of NO Gamma, Beta, and Epsilon bands.

Run 8011's order II spectrum of the NO Gamma System's (0,2) band was fit with an order I wavelength scale and a normalized and background-corrected signal strength scale. Figure 31 shows an overlay of the EBFNO prediction with the spectrometer/array detector spectrum. The rotational and vibrational temperatures used in this prediction were 400 K and 1,200 K, respectively. The shape of the spectrum was relatively insensitive to the value of vibrational temperature over the range of values

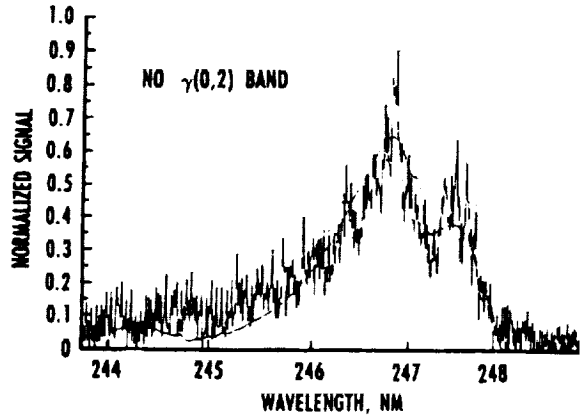

Fig. 31. NO experimental and model spectra for Run 8011.

possible for the tunnel conditions. The shape was, however, rather sensitive to the rotational temperature value. Overall, the 400 K value provided the best fit to the spectrum. It is believed that a much better fit could be achieved if time were available to fine tune spectrometer/array detector parameters and to account for spectral sensitivity variation over the wavelength and physical pixel region utilized. This measurement's uncertainty is a standard deviation of 50 K.

SUMMARY

The measurements obtained are summarized in Table 3. Numerous self-emitting metallic species were identified, many of which may be associated with an aging/erosion process within the B30HST. Because there were only 16 tunnel runs, it was only possible to obtain spectral measurements over a limited range of wavelengths and time sampling periods. Many spectral features of the flow remain uninvestigated. Because flow self-emission is important to all optical diagnostic techniques, it is recommended that additional spectral studies be performed.

The three electron beam-excited species that were identified are nitrogen, helium, and nitric oxide. The high metallic radiation background interfered with attempts to obtain the time-wise variation of N_2 density and He radiation with the optical filter/PMT channels. In the case of the N_2 density measurements the result of interference was increased uncertainty. Unfortunately, the interference caused the time-wise He measurement to fail completely. It is recommended that the electron beam be modulated to provide discrimination against the background radiation in future N_2 density measurements. Careful data reduction produced useful measurements of N_2 vibrational temperature, even though the high background from metallic species significantly increased measurement uncertainty. Perhaps the recommended additional spectral studies would reveal N_2^+ First Negative System band-pair regions having less background. Detection of the He arrival (see Fig. 20) was easily accomplished with the spectrometer/array detector system. Because of this, it is recommended that this means of detecting He arrival be used in the future. With proper calibrations of the system an He number density could be obtained. Although the flow conditions were out of limits for the run in which the NO spectrum was recorded, the usefulness of the NO spectrum for determination of free-stream rotational temperature was demonstrated and should be exploited in future experiments. Indeed, based on the strong NO signals, it is recommended that lower resolution NO spectra be obtained to provide a measure of NO vibrational temperature in the same manner that the N_2 vibrational temperature was obtained.

REFERENCES

1. Neumann, R. D. "Requirements in the 1990's for High Enthalpy Ground Test Facilities for CFD Validation." 16th Aerodynamic Ground Testing Conference, Seattle, WA, June 18-20, 1990, AIAA Paper 90-1401.

2. Boeing Defense & Space Group, Military Airplanes Division. "Reacting Gas Experimental Data in Low Density Flow. Task I. Boeing 30 Inch Hypersonic Shock Tunnel Nozzle Experimental Survey." WRDC-TR-90-3010, May, 1990.

Table 3. Results

MEASUREMENT	RESULTS
SELF-EMITTING RADIATIVE SPECIES	ALUMINUM, CHROMIUM, COPPER, IRON, MANGANESE AND ALUMINUM OXIDE WERE DETECTED. LIGHT FROM THESE METALLIC SPECIES WAS GENERATED AT HIGH TEMPERATURE UPSTREAM OF THE NOZZLE THROAT, AND WAS PROBABLY REFLECTED BY SURFACES DOWNSTREAM OF THE THROAT INTO THE DETECTORS.
ELECTRON BEAM-EXCITED RADIATIVE SPECIES	NITROGEN, HELIUM, AND NITRIC OXIDE SPECTRA WERE RECORDED. NO APPEARED AT THE BEGINNING OF THE USABLE FLOW PERIOD, N_2 DURING THE PERIOD, AND He AFTER THE PERIOD.
NITROGEN DENSITY	AIR DENSITY VALUES FELL BETWEEN FROZEN AND EQUILIBRIUM PREDICTIONS, AS EXPECTED (SEE FIGS. 21 AND 22). STRONG BACKGROUND LIGHT FROM METALLIC SPECIES AFFECTED THE MEASUREMENTS.
NITROGEN VIBRATIONAL TEMPERATURE	THREE MEASUREMENTS WERE ACQUIRED. THE N_2^+ FIRST NEGATIVE SYSTEM (0,1) AND (1,2) BANDS WERE USED. METALLIC BACKGROUND LIGHT CAUSED LOW SIGNAL TO NOISE CONDITIONS. THE AVERAGE VIBRATIONAL TEMPERATURE WAS 1240K WITH A STANDARD DEVIATION UNCERTAINTY OF 50K.
HELIUM (DRIVER GAS) ARRIVAL TIME	SPECTROMETER/ARRAY DETECTOR MEASUREMENTS OF THE He ARRIVAL TIME INDICATED THE CHEMICALLY PURE TEST TIME RANGED BETWEEN 1.0 AND 2.4 MSEC. STRONG METALLIC LIGHT PREVENTED MEASUREMENT BY OPTICAL FILTER/PMT CHANNELS.
NITRIC OXIDE FREE-STREAM ROTATIONAL TEMPERATURE	THE NO ROTATIONAL TEMPERATURE WAS 400K WITH A STANDARD DEVIATION UNCERTAINTY OF 50K. THIS RUN'S FLOW CONDITIONS WERE OUT OF LIMITS BECAUSE OF PREMATURE DIAPHRAGM RUPTURE.

3. Cassady, P. E. and Lieberg, S. F. "Planar Laser Induced Fluorescence Measurements in Hypersonic Shock Tunnel Flow." 21st Fluid Dynamics, Plasma Dynamics and Lasers Conference, Seattle, WA, June 18-20, 1990, AIAA Paper 90-1549.

4. Shelton, D. P. and Cassady, P. E. "Electron Beam Density Measurement in a Hypersonic Shock Tunnel Flowfield." 17th Aerospace Ground Testing Conference, Nashville, TN, July 6-8, 1992, AIAA Paper 92-3933.

5. Muntz, E. P. "The Electron Beam Fluorescence Technique." AGARDograph 132, December 1968.

6. Center, R. E. "Plural and Multiple Scattering of Fast Electrons in Gases." *Physics of Fluids*, Vol. 13, No. 1, January 1970, p. 79.